

Washington University in St. Louis

Washington University Open Scholarship

McKelvey School of Engineering Theses & Dissertations

McKelvey School of Engineering

Spring 5-14-2019

Fracture Toughness Improvement of Ceramics by Grain Size Control and Ductile Phase Reinforcement

Kesong Wang

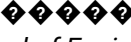
Washington University in St. Louis

Follow this and additional works at: https://openscholarship.wustl.edu/eng_etds



Part of the [Ceramic Materials Commons](#), [Other Materials Science and Engineering Commons](#), and the [Other Mechanical Engineering Commons](#)

Recommended Citation

Wang, Kesong, "Fracture Toughness Improvement of  Ceramics by Grain Size Control and Ductile Phase Reinforcement" (2019). *McKelvey School of Engineering Theses & Dissertations*. 423. https://openscholarship.wustl.edu/eng_etds/423

This Thesis is brought to you for free and open access by the McKelvey School of Engineering at Washington University Open Scholarship. It has been accepted for inclusion in McKelvey School of Engineering Theses & Dissertations by an authorized administrator of Washington University Open Scholarship. For more information, please contact digital@wumail.wustl.edu.

WASHINGTON UNIVERSITY IN ST. LOUIS
School of Engineering and Applied Science
Department of Mechanical Engineering

Thesis Examination Committee:
Dr. Shankar Sastry
Dr. Kathy Flores
Dr. Peng Bai

Fracture Toughness Improvement of **Al₂O₃** Ceramics by Grain Size Control and
Ductile Phase Reinforcement

by

Kesong Wang

A thesis presented to the School of Engineering
of Washington University in St. Louis in partial fulfillment of the
requirements for the degree of
Master of Science

May 2019

Saint Louis, Missouri

Contents

List of figures	iii
List of tables	iii
Acknowledgments (Required).....	iv
Dedication (Optional).....	v
Abstract (Optional)	vi
1 Introduction	1
2 Background	2
2.1 Use of nano-Oxide Ceramics	2
2.2 Al_2O_3 based ceramic structure and properties	2
2.3 Ductile Phase Reinforcement.....	3
2.4 Electroless Nickel Plating (ENP)	5
2.5 Spark Plasma Sintering	6
2.6 Thermal Etching.....	8
3 Research Objectives	9
4 Experimental Procedure	10
4.1 Materials.....	10
4.2 Nano particle Preparation.....	10
4.3 Electroless Nickel Plating	11
4.4 Consolidation by Spark Plasma Sintering.....	12
4.5 Mechanical Property Measurement	13
4.5.1 Vickers Hardness Number.....	13
4.5.2 Fracture Toughness.....	14
4.6 Post Spark Plasma Sintering Annealing	16
4.7 Microstructure Observation	16
5 Results and Discussion	17
5.1 Microstructures	17
5.1.1 Microstructure of powders.....	17
5.1.2 Microstructure of consolidated SPS	23
5.2 Indentation	27
5.3 Densities	29
5.4 Hardness	31
5.5 Fracture Toughness	33

6 Summary and Conclusions	35
7 Future Work	36
References	37

List of tables

Table 4.1: Typical Combined Sn/Pd Catalyzing Bath.....	11
Table 4.2: Bath Composition for Electroless Nickel Plating Using Sulfate Bath.....	11
Table 4.3: Bath Composition for Electroless Nickel Plating Using Chloride Bath	12
Table 5.1: Density of consolidated coated and uncoated alumina.....	30
Table 5.2: Hardness of coated and uncoated alumina	31
Table 5.3: Fracture toughness of all uncoated and coated samples.....	33

List of figures

Figure 2.1: Alumina chemical structure	3
Figure 2.2: Schematic demonstration	4
Figure 2.3: Basic stages of SPS process.....	7
Figure 2.4: Etching techniques used in ceramography	8
Figure 4.1: Schematic diagram of hardness test.....	14
Figure 4.2: Indentation for fracture toughness calculation	15
Figure 5.1: Transmission electron microscopy (TEM) of alumina (200nm scale)	17
Figure 5.2: 5.2 (a) uncoated alumina 100 nm, (b) uncoated alumina 0.5-1 μm (c) uncoated alumina 10 μm	18
Figure 5.3: EDX spectrum of nickel coated 0.5-1 μm alumina	19
Figure 5.4: Elemental mapping of 0.5-1 μm coated alumina.....	20
Figure 5.5: Element distribution of 0.5-1 μm coated alumina	21
Figure 5.6: Elemental mapping of 100 nm coated alumina	22
Figure 5.7: SEM micrograph of 10 μm coated alumina	23
Figure 5.8: SEM micrograph of 100 nm coated alumina annealed for 10 hrs (magnification: 5000x).....	24
Figure 5.9: EDX spectrum and element distribution of 100 nm coated alumina annealed for 10 hrs	25
Figure 5.10: SEM micrograph of 100 nm coated alumina annealed for 1.5 hrs (magnification: 10000).....	26
Figure 5.11: EDX spectrum of 100 nm coated alumina annealed for 1.5 hrs	27
Figure 5.12: (a) Optical micrograph of indentation of 100 nm coated alumina sintered at 1325°C (b) Optical micrograph of indentation of 100 nm uncoated alumina sintered at 1325°C.....	28
Figure 5.13: Optical micrograph of indentation of 100 nm coated alumina sintered at 1400 °C.....	29

Acknowledgments

My deepest gratitude goes first and foremost to Prof. Sastry, my supervisor, for his constant encouragement and guidance. He has walked me through all the stages of my research and the writing. Without his consistent and illuminating instruction, this thesis could not have reached its present form.

Second, I would like to express my heartfelt gratitude to Kunlong Jia and Yinhui Ye who led me into the research lab and experiment and guided me for the requirements and procedures of our research.

Last my thanks would go to Dr. George Li for help with the SPS Nano ceramics in consolidation experiments.

Kesong Wang

Washington University in St. Louis

May 2019

Dedicated to my parents.

Additionally, I am deeply indebted to my beloved family for their loving considerations and great confidence in me all through these years. Thanks to them for financing me to complete my master's degree in mechanical engineering.

ABSTRACT OF THE THESIS

Fracture Toughness Improvement of Al_2O_3 Ceramics by Grain Size Control and
Ductile Phase Reinforcement

by

Kesong Wang

Master of Science in Mechanical Engineering

Washington University in St. Louis, 2019

Research Advisor: Professor Shankar Sastry

This study used grain size control and ductile phase reinforcement to improve fracture toughness of Al_2O_3 ceramics. Alpha alumina particles of 100 nm, 0.5-1 micrometers, and 10 micrometers were coated with 1-5 nm nickel by electroless nickel plating (ENP). The coated powders were consolidated at 1200°C-1500°C by spark plasma sintering (SPS). The sintered samples were annealed at 1100 °C for 1.5 hours and 10 hours to determine the effect of post sintering annealing on hardness and fracture toughness. Density of the samples were measured by the standard Archimedes method using a 5 mL pycnometer. Hardness values were determined by Vickers micro hardness indentations and the fracture toughness values were calculated from indentation dimensions and indentation-tip crack length measurements. Uncoated powders, coated powders, consolidated samples and post SPS annealed samples were characterized by Scanning Electron Microscopy (SEM). The fracture toughness of alumina increased by more than 100% (9.19 $\text{MPa}\cdot\sqrt{\text{m}}$ for coated alumina in comparison to about 3.98 $\text{MPa}\cdot\sqrt{\text{m}}$ for uncoated alumina) for certain particle size-coating-sintering conditions. Results were analyzed in terms of crack bridging mechanisms.

Chapter 1

Introduction

In recent years, ceramic materials have been widely used in foodstuff fields, chemical industry, biomedical applications, electronic applications, thermal barrier coatings, and for environmental protection due to their ability to resist high temperatures, severe chemical environment and high mechanical strength [1-4]. Alumina is one of the most important materials due to its durability, high temperature stability and chemical resistance [5]. However, alumina is a brittle material and its fracture toughness is very low [6]. The spark plasma sintering is a new technology that available for improvement of fracture toughness of ceramics [7]. And previous research has proved that SPS is capable for fracture toughening of alumina [8]. Our objective is to determine the relationship between material variables (particle size, grain size, and coating thickness) process variables (sintering temperature and time, post sintering annealing), and material properties (% relative density, hardness, and fracture toughness) for alumina based ceramics. Several different temperatures were used as sintering temperature for each alumina particle size. Then the fracture toughness was compared. Also at each temperature, different particle size of coated alumina was sintered to learn the effect of **Al₂O₃** particle size on the mechanical property of alumina ceramic. In addition, thermal etching is an important method for developing the microstructures of **Al₂O₃** and **ZrO₂** ceramics [9, 10]. A new approach to study the effect of thermal etching by revealing the location of grain boundaries under polished sample surface was used to determine the feasibility of fracture toughness improvement of **Al₂O₃**.

Chapter 2

Background

2.1 Use of Nano-Oxide Ceramics

Nano-Oxide ceramics are high-tech materials that have diverse applications in engineering, medicine, and industrial production. The need for tough, strong and stable ceramics is met by either Nano-alumina and Nano-zirconia based ceramics and composites or other oxide ceramics [11]. The amorphous nano alumina powder can be used as an active catalyst in the transesterification reaction for biodiesel production for industrial use. Also sintered nano ceramic powders will have lower porosity, which majorly contributes to the brittleness of ceramics. Thus the fracture toughness can be enhanced.

2.2 Al_2O_3 based ceramic structure and properties

Alumina, often called as aluminum oxide, is a chemical compound composed of oxygen and aluminum atoms and connected by covalent bonding.

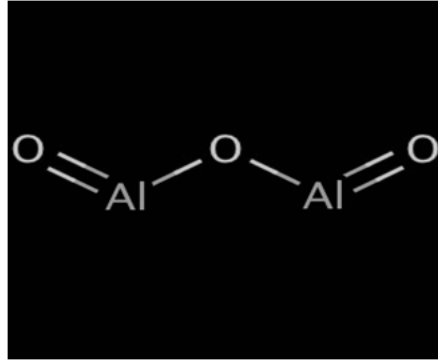


Fig. 2.1 Alumina chemical structure

Alumina occurs in several other forms. And the most common and naturally occurring form is Corundum. Oxygen atoms form a slightly distorted hexagon in the lattice of corundum, which is found as a mineral in genesis and some other marbles. The alumina is also found in nepheline syenite.

Alumina, as crystalline ceramic, has complex crystal structures along with strong, directional, covalent atomic bonding. Those strong covalent bondings prevent the dislocation of alumina atoms which can lead to permanent deformation for metallic materials. Therefore, the interatomic bonds will break before dislocations happen when the maximum stress of alumina is loaded. Then crack propagation occurs. The absence of plastic deformation is termed as brittle fracture [12]. Based on its structure, alumina has very good electrical insulation and possesses good thermal conductivity. Alumina also has very high stiffness and compressive strength (2000-4000 MPa) and hardness (15-19 GPa). In addition, high corrosion and wear resistance are also advantages of alumina.

2.3 Ductile Phase Reinforcement

The toughening brittle solids through the incorporation of a ductile phase attract considerable attention of scientists in an attempt to enhance the ductility and fracture toughness of intermetallic and ceramic [13-24]. The toughening is approached by the reinforcement phase that can be made to intercept crack. Catastrophic fracture can be impeded through the formation of ductile-phase

ligaments bridging the crack wake. The formative crack bridging and plastic deformation of the particles together with crack deflection [25] at the particle, crack blunting, and interfacial debonding result additional toughening. The extent of toughening can be expressed as:

$$\Delta G_c = f \sigma_y r \chi \quad (2.1)$$

Where:

ΔG_c = The increase in fracture energy

f = The area fraction

σ_y = Individual yield strength

r = A representative cross-sectional radius

X = Dimensionless function representing the work of rupture which can vary between ~ 0.5 and ~ 8 (depending upon the degree of interface debonding and constitutive properties of the reinforcement phase [16-20]).

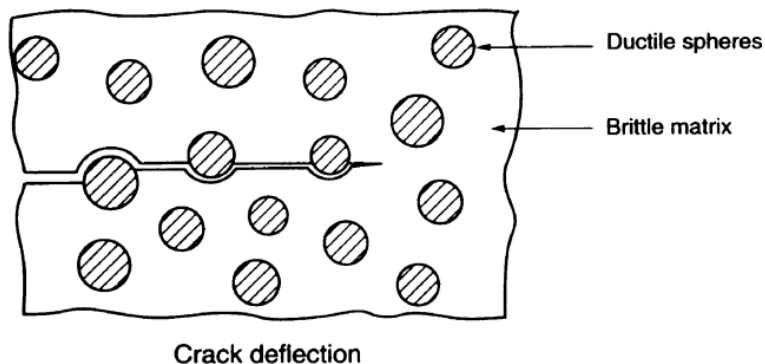


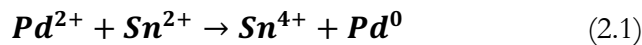
Fig 2.2 Schematic demonstration

This approach has been used successfully in several ceramic/metal and intermetallic/metal systems, including glass/Al, glass/Ni, Al₂O₃/Al, WC/Co, TiAl/Nb, TiAl/TiNb, and Nb₅Si₃/Nb [13-24].

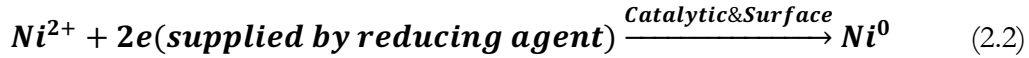
2.4 Electroless Nickel Plating (ENP)

Electroless nickel plating is an autocatalytic reaction deposit nickel layer on another solid material's surface, like metal, plastic, and ceramics. The process includes dissolution of the the element to be deposited into a solution-the bath of plating, where a reducing agent reacts with the material's ions to reduce metal ions and deposit the nickel ions [26]. Unlike electro plating, electroless nickel plating has many advantages. For example, electroless nickel plating prevents corrosion and wear since there is no current through the plating solution during the reaction. And electroless nickel plating can plate an even layer outside the corresponding shape of the material. Electroless nickel plating can even coating on nano particles using nano powder in the plating bath.

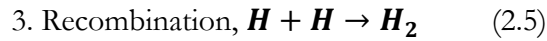
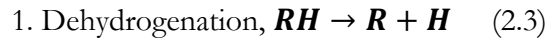
In the process of electroless thin-nickel-film deposition, uniform film thickness is reached. The density of nucleation sites on the catalyzed substrate determines the properties of the final produced films. During plating a continuous film of uniform thickness results, the film uniformity and thickness are determined by the density of nucleation. The density and thickness of nickel coating are time dependent functions during the reaction period in the plating bath. In order to catalyze the reaction, a sensitizer, usually **SnCl₂**, and catalyst, thiourea should be used during the reaction [27]. During the sensitization and catalyzing terms, ions or molecules are absorbed from solutions such as acidic Sn (II) and/or Sn (IV). During this process, the active metal in the catalyst solution, usually **PdCl₂**, can be reduced to palladium by the sensitizing ion, a simplified reaction function can be presented as: [28]



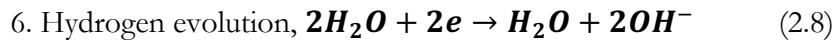
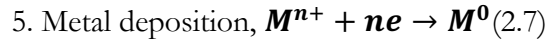
This electroless nickel plating process involves a continuous buildup of nickel coating on a substrate in an appropriate aqueous solution. A reducing agent in solution is used to supply the electrons to convert nickel ions to nickel,



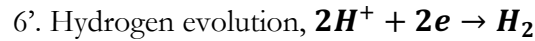
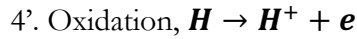
According to Van DenMeerakker [29], electroless deposition processes may be referred to a universal electrochemical mechanism regardless of the possible nature of the reducing agents R. The process is made up of a series of anodic and cathodic reaction. With considering there are two kind of solution bath, acid bath and alkaline bath, the process can be simplified as the following,



For alkaline media bath, the following two cathodic stages are:



For acid media bath, stages 4 and 6 should be as follow:



For electroless nickel plating, the metal deposition is nickel deposition. Thus, electroless nickel plating can be considered as two independent electrode reaction: anodic partial reaction and cathodic partial reaction.

2.5 Spark Plasma Sintering

The spark plasma sintering was used in this experiment because the alumina powders can be fully densified at a much lower temperature and a much shorter time than in conventional sintering process. The SPS is a newly developed rapid sintering technique with a great potential for achieving fast densification results with minimal grain growth in a short sintering time.

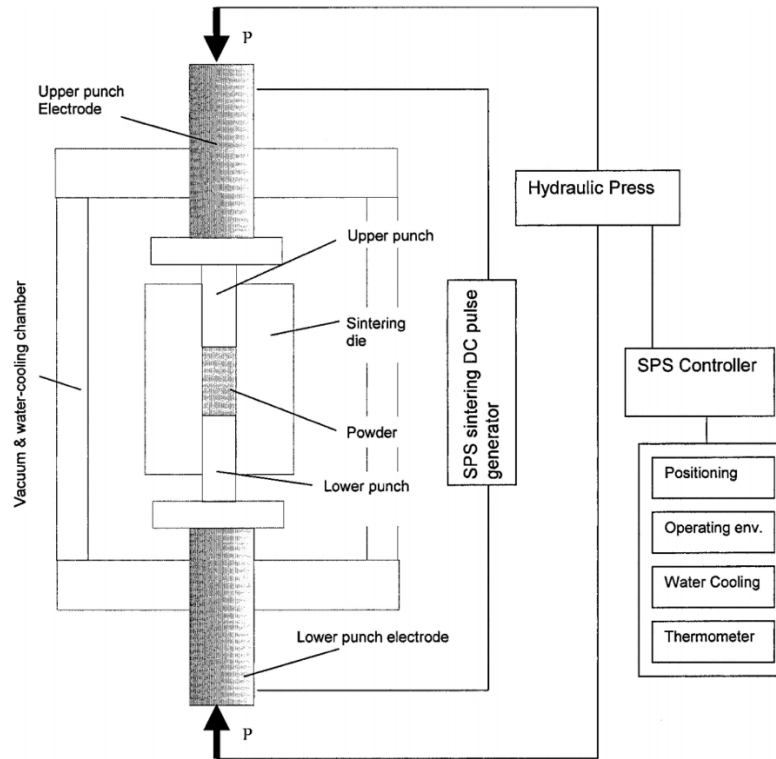


Fig 2.3: Basic stages of SPS process [30]

The basic SPS technique uses pulsed electrical current combined with rapid heating and applied pressure in order to achieve fully densified compact in a short time. The principle of SPS process is shown in Fig. 2.3[30]. The sintered powder is directly loaded in a graphite die. The punches are also made from graphite. The material of graphite dies and punches limits the applied external pressure under 100 MPa during the sintering process.

The process starts with initial activation by apply a pulsed current, later the densification process takes place by the applied external pressure when the proposed activation level is achieved. Pulse discharge is normally achieved by applied voltage about 30 V and a current about 600-1000 A. The electrical discharges across sample may generate plasma/spark. The surface layers of powder particles are subjected in a plasma environment. This process prevents the oxide layers, surface impurities, and absorbents, which are residual products on surface of the powder particles [30].

2.6 Thermal Etching

The microstructure plays an important role on ceramics' performance. Refinement of the microstructure of ceramics is an attractive method to improve properties of ceramics. The preparation of ceramographic specimens consists five broad steps: sawing, embedding, grinding, polishing and etching. Among those, etching reveals and delineates grain boundaries and other microstructure features that are not as apparent as polish on the surface. The etching preparation can be divided into branches in Fig. 2.4[31,32]:

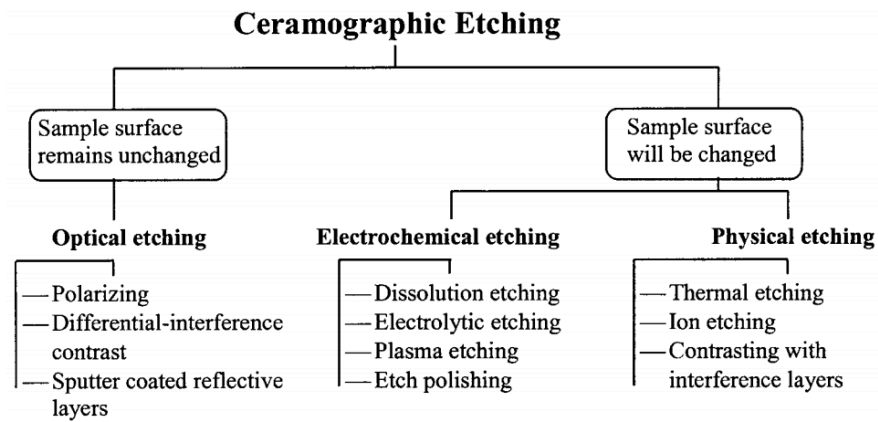


Fig. 2.4 Etching techniques used in ceramography[31,32]

Thermal etching has received wide acceptance among available etching techniques. The technique used for alumina involves heating a polished sample in a furnace for 15 minutes to couple hours at temperature of 150 °C below the sintering temperature [33].

Chapter 3

Research Objectives

The goal of our study is to determine the feasibility of improving the fracture toughness of alumina based ceramics. To realize this goal, we have used electroless nickel plating and spark plasma sintering to produce ductile phase reinforced **Al₂O₃** and have carried out a systematic investigation of the relationship between material and process parameters. The specific objectives of current investigation are:

- Determine the feasibility of producing uniform ductile nickel coating on 100-10000 nm **Al₂O₃** particles.
- Produce fully dense compacts of Ni-coated **Al₂O₃** by spark plasma sintering.
- Determine density, hardness, and fracture toughness of SPS processed and post SPS annealed samples.
- Evaluate the effectiveness of combined fine grain size and ductile phase on hardness and fracture toughness improvement of **Al₂O₃** ceramics.

Chapter 4

Experimental Procedure

4.1 Materials

Our particles of 10 μm 100% alpha phase alumina powder, 0.5~1 μm ultrapure alumina powder, and 100 nm 99.99% alpha phase alumina powder were purchased from Inframat Advanced Nanomaterials. The chemicals used for sensitization, catalysis, and electroless nickel plating bath were purchased from SIGMA-ALDRICH, which now is Millipore SiGMA. And the water used for making all bath solutions was deionized nanopore water.

4.2 Nano particle Preparation

20 g alumina powder particles were weighted on balance with precision of 0.01 mg each time. Some powder particles were bagged in seal plastic bags and sent to SPS directly as uncoated samples. Powder particles prepared for coated samples, were first rinsed with deionized water. Then the sensitizer, **SnCl_2** , and hydrochloric acid were added. The mixture was allowed to settle for 30 minues for sensitizing. After sensitizing, catalyst **PdCl_2** was added and rinsed with nano deionized water. The constituents and quantity were listed in table 4.1.

Table 4.1 Typical Combined Sn/Pd Catalyzing Bath

Chemical	Quantity
SnCl₂	2 g/L
PdCl₂	0.2 g/L
HCl	10 ml/L

4.3 Electroless Nickel Plating

After the alumina powder particles were prepared, the bath solution of electroless nickel plating needed to be prepared. For electroless nickel plating, we have two kinds of bath: sulfate bath and chloride bath. Different recipes were used for the two baths.

For the sulfate bath, nickel sulfate serves as nickel ion source for plating. And the pH value of the solution was kept at 5.4, 1 g/L sodium hydroxide was added to maintain the pH value. The solution bath needed to be heated to around 85°C on hotplate/stirrer before the prepared powder particles was added into the bath solution. During the reaction, the powder particles were kept dispersed by an ultrasonic bar inserted into the bath and stirred by a magnetic stir bar. After the reaction, the coated particles were washed by Nano deionized water for three times until the solution was colorless. For each time, we need to wait the particles to deposit before wash. Then the particles were waited to be dried. The composition of the plating bath solution is listed in table 4.2.

Table 4.2 Bath Composition for Electroless Nickel Plating Using Sulfate Bath

Constituents	Concentration
Nickel Sulfate	30 g/L
Sodium Citrate	24 g/L
Ammonium Phosphate	45 g/L
Sodium Hypophosphate	40 g/L
Thiourea	0.1 g/L

For the chloride bath, the pH value and reaction temperature are the same with sulfate bath. The nickel comes from nickel chloride. The composition of the chloride bath is listed in table 4.3.

Table 4.3 Bath Composition for Electroless Nickel Plating Using Chloride Bath

Constituents	Concentration
Nickel Chloride	35 g/L
Sodium Citrate	24 g/L
Ammonium Chloride	40 g/L
Sodium Hypophosphate	40 g/L

4.4 Consolidation by Spark Plasma Sintering

Spark plasma sintering consolidation procedure was carried out at SPS Nano Ceramic. The prepared powder particles were sintered in a furnace with maximum capacity of 100 kW. It can produce DC current up to 10000 A and DC voltage of 10 V. The hydraulic press capacity is 10 T. The sintering temperature can go up to 2300°C. The vacuum environment is 5 Pa.

The powder particle sample was placed in a cylindrical die, lined with graphite sheet which facilitates easy removal of the sintered compact. Then, the time and temperature of sintering were set, the required vacuum atmospheres inside the chamber was achieved with a vacuum pump. Required load and power were set to auto mode. Also, set the z-axis position to zero. The temperature during the sintering was measure by pyrometer. High DC Pulse passed through graphite electrodes and heated the graphite molds, which in turn instantaneously heated the powder sample by Joule-heating. The sparking among the particles of sintered powder sample leads to the faster heat and mass transfer. The sintering is completed in a short time about 5 mins. The short period of SPS minimize the grain coarsing and results in high-density compact of consolidated sample. For uncoated alumina, the powders were sintered at 1325°C and 1400°C. For coated alumina, the powders were sintered at 1200°C, 1250°C, 1325°C and 1400°C. The sintered compact is about 6 mm for height and 20 mm for diameter. Then the compact was cut and polished for Vickers hardness test.

4.5 Mechanical Property Measurement

To determine the mechanical property of consolidated samples, two values of sample needed to be calculated: hardness number and fracture toughness.

4.5.1 Vickers Hardness Number

The Vickers hardness number was measured by a Phase II Vickers Hardness Tester. An indentation should be left after the sample was pressed by the indenter under certain load. The maximum load of the tester is 50 kg with lower loads of 30 kg, 20kg, 10kg, and 1 kg. Three to four indentations were made on each sintered sample by Vickers Hardness Tester to determine the hardness number. The equation to calculate Vickers microhardness is:

$$Hv = \frac{1.8544F}{d^2} \quad (4.1)$$

Where:

F=load (kgf)

d=length of indentation diagonal line (mm)

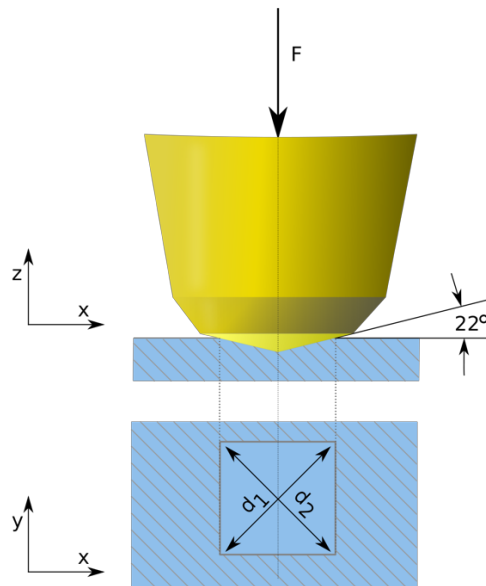


Fig. 4.1 Schematic diagram of hardness test

4.5.2 Fracture Toughness

The fracture toughness values were calculated using the experimental procedure commonly followed in indentation tests [34], the procedure consists of relating the lengths of the cracks shown in figure 4.2, growing in corners of the Vickers indentation when a load (P) is applied, with the toughness of the material.

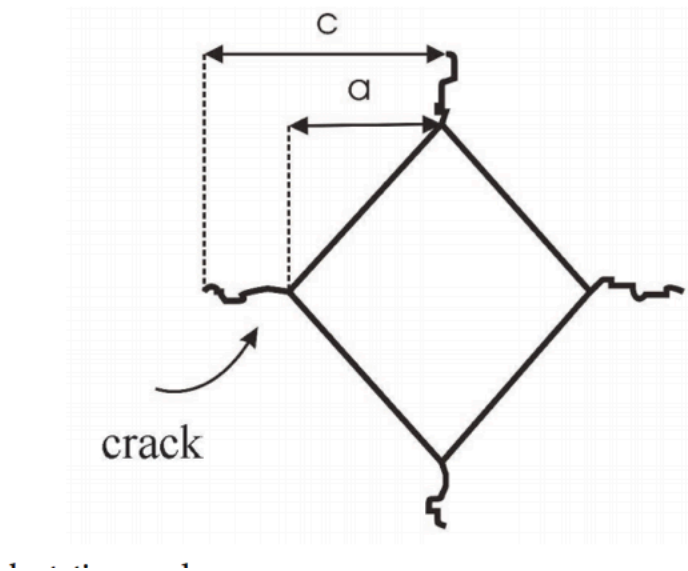


Fig. 4.2 Indentation for fracture toughness calculation [34]

To calculate fracture toughness by this method, one of the most commonly used equations is:

$$K_{IC} = 0.16 \left(\frac{c}{a} \right)^{-1.5} (H a^2)^{1/2} \quad (4.2)$$

Where:

K_{IC} = Fracture toughness (MPa m^{1/2})

H = Vickers hardness (MPa)

c= Average length of the cracks obtained in the tips of the Vickers marks (mm)

a=Half average length of the diagonal of the Vickers marks (mm)

4.6 Post Spark Plasma Sintering Annealing

The coated and uncoated sintered samples were annealed in a **Thermolyne™** Benchtop 1100°C Muffle Furnace. The voltage of the furnace is 240 V. The furnace is capable to heat samples from 100°C to 1100°C. The consolidated sample was inserted into the furnace and the door of furnace was closed. The temperature on the small screen was set to specified temperature and the furnace begins to heat up while the green light is on. It takes about one and a half hours for the furnace to heat to 1100 °C. Two annealing time of 1.5 hours and 10 hours were tested. After 1.5 hours after the temperature reach the specific temperature, take one of each annealing sample out and cool down. After 10 hours after the temperature reach the desired temperature, take other samples out and cool down. The color of coated sample changed to green after annealing. And then test the hardness and fracture toughness of annealed sample again to compare the values with that before annealing.

4.7 Microstructure Observation

All the samples after indentation test were taken to take pictures of indentation by optical microscope. From microscope we can see crack clearly on samples. After that, all the samples were taken to IMSE department and NRF of Washington University in St. Louis for SEM. Under SEM, we can see the grain boundaries clearly and determine the grain size. Also chemical analysis and mapping were done by the SEM machine.

Chapter 5

Results and Discussion

5.1 Microstructures

5.1.1 Microstructure of powders

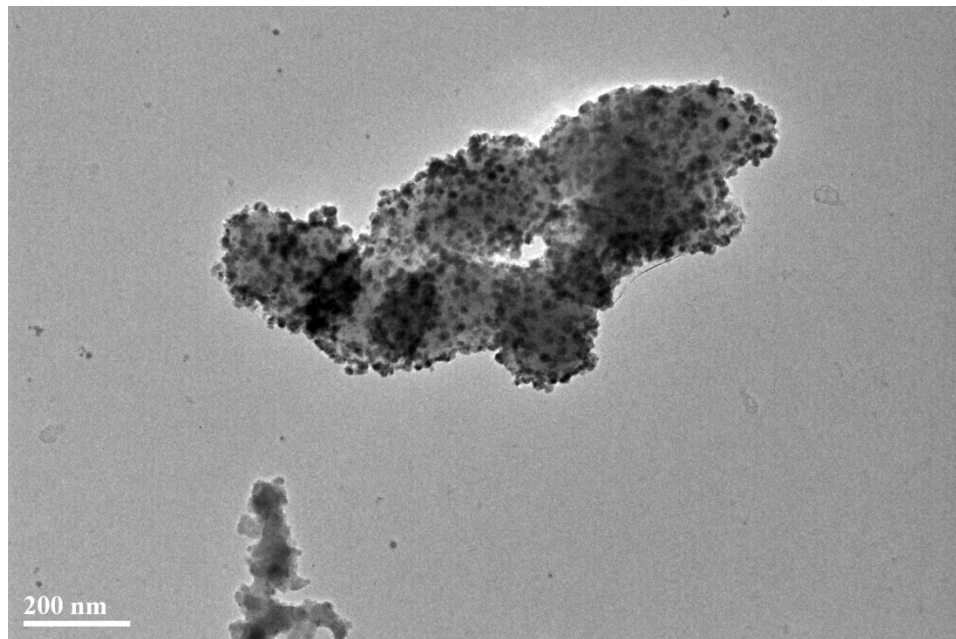
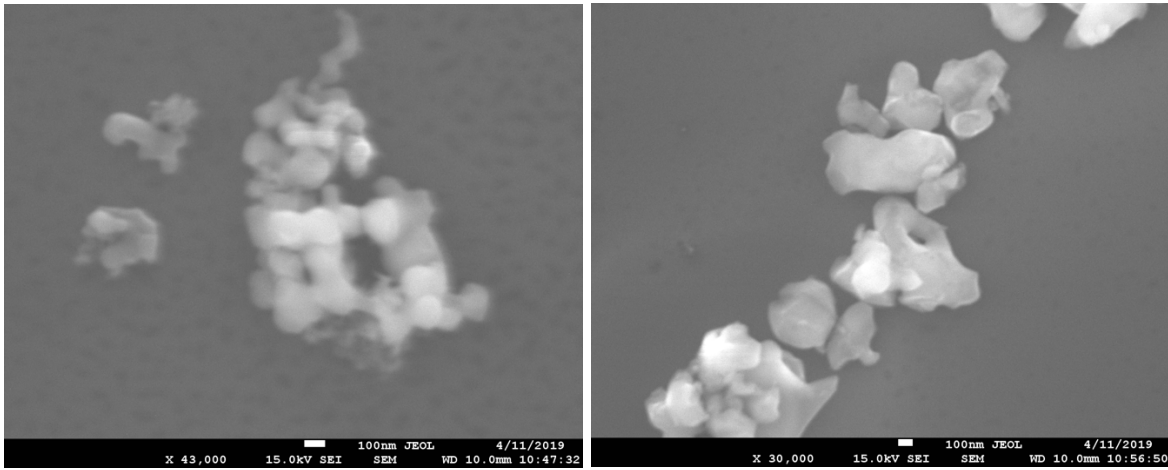


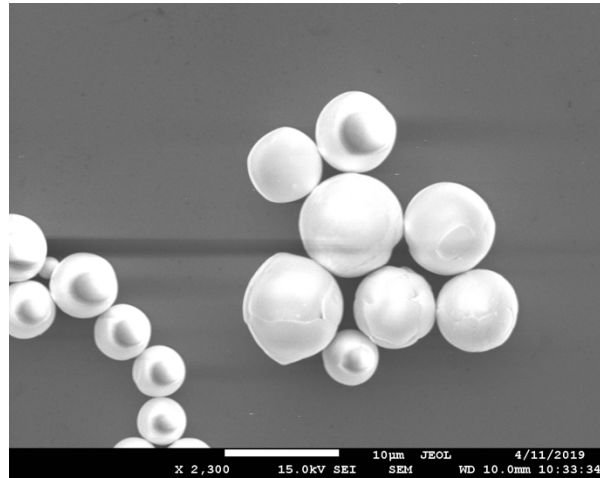
Fig. 5.1 Transmission electron microscopy (TEM) of alumina (200nm scale)

From fig 5.1, we can see the particle size is around 100 nm. The black particles around alumina are palladium with nickel coating around them.



(a)

(b)



(c)

Fig 5.2 (a) uncoated alumina 100 nm (b) uncoated alumina 0.5-1 μm (c) uncoated alumina 10 μm

Fig 5.2 shows the uncoated particles correspond with the particle sizes shown on the chemical labels.

Electron Image 4

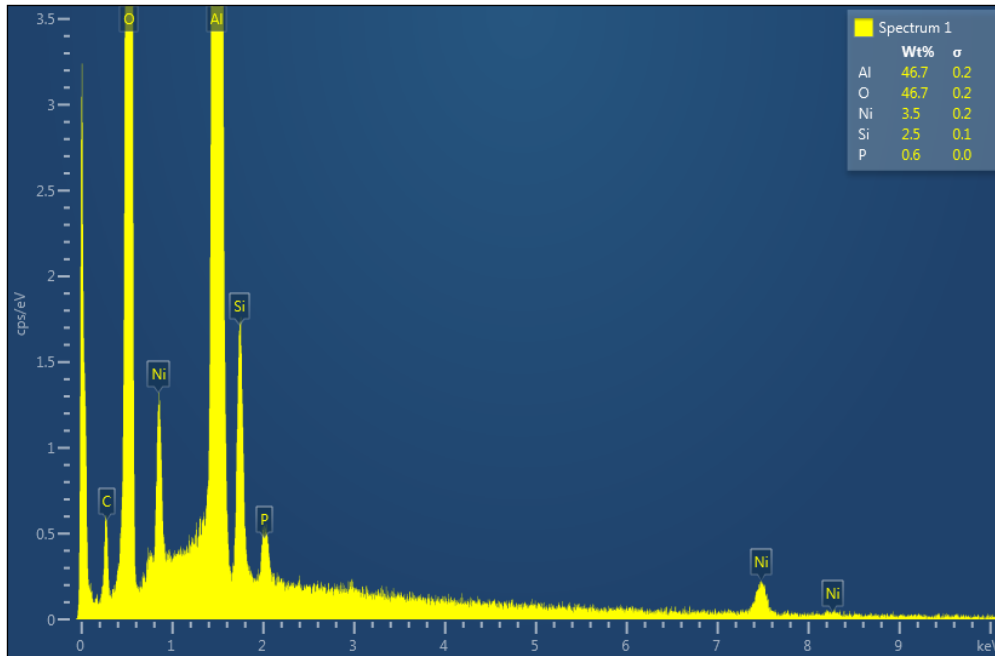
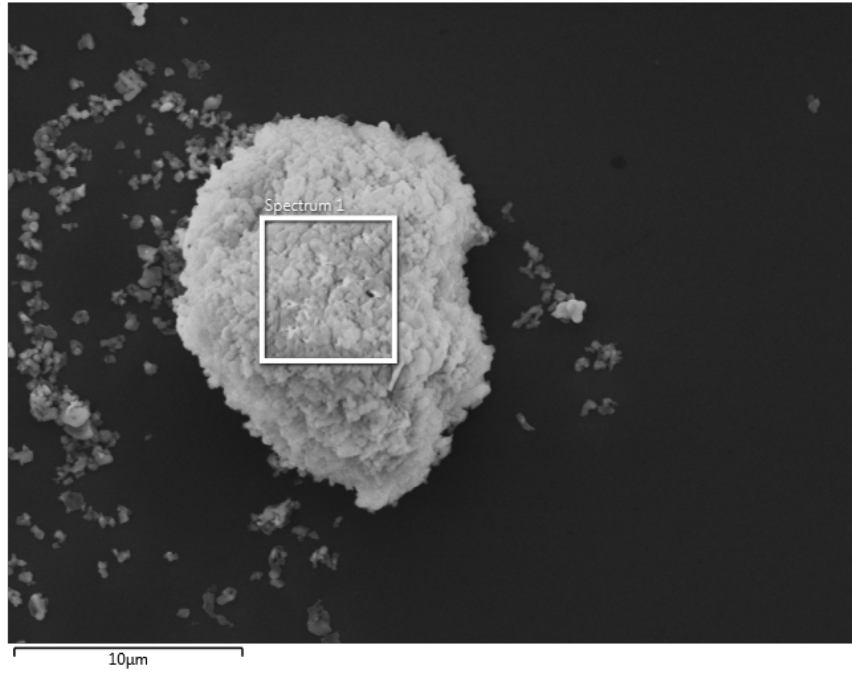


Fig 5.3 EDX spectrum of nickel coated 0.5-1 µm alumina

The spectrum in fig 5.3 is analyzed in the region inside of the white box shown in fig 5.3. The spectrum shows that this region has nickel element and occupy 3% of weight. Presence of nickel was proved by $K\alpha$ peaks presenting on the spectrum. $K\alpha$ peaks of other major elements also shown in Fig 5.3 with proper weight percent as predicted.

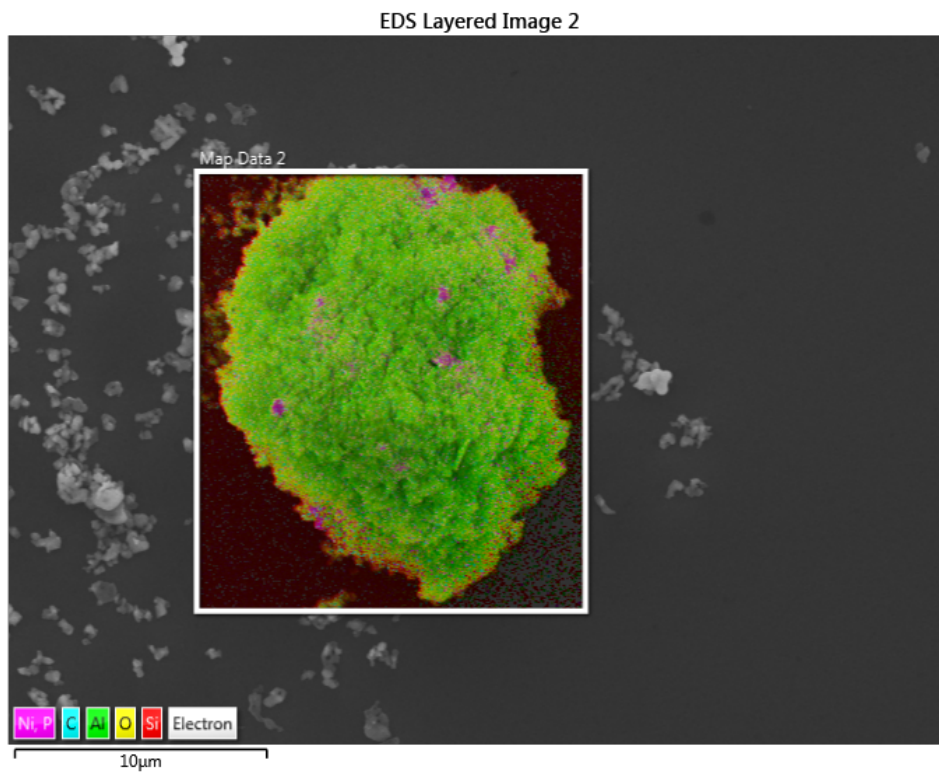


Fig 5.4 Elemental mapping of 0.5-1 μ m coated alumina

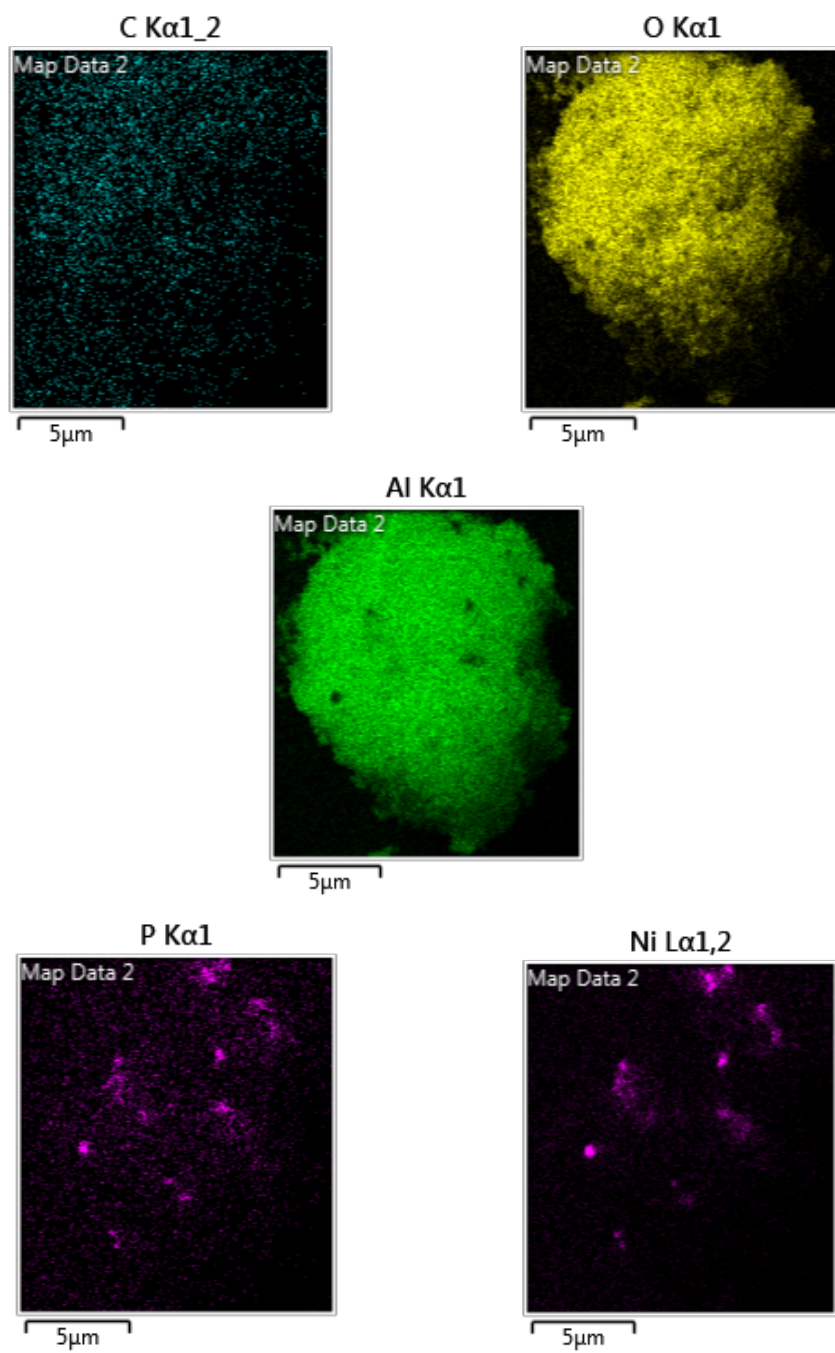


Fig 5.5 Element distribution of 0.5-1 μm coated alumina

Fig 5.4 and fig 5.5 indicates that the nickel plating was successful for 0.5-1 μm alumina. Although nickel signals are distributed all over the tested region, there are a few concentrated spots on the elemental mapping, which indicates that the coating may not be uniform.

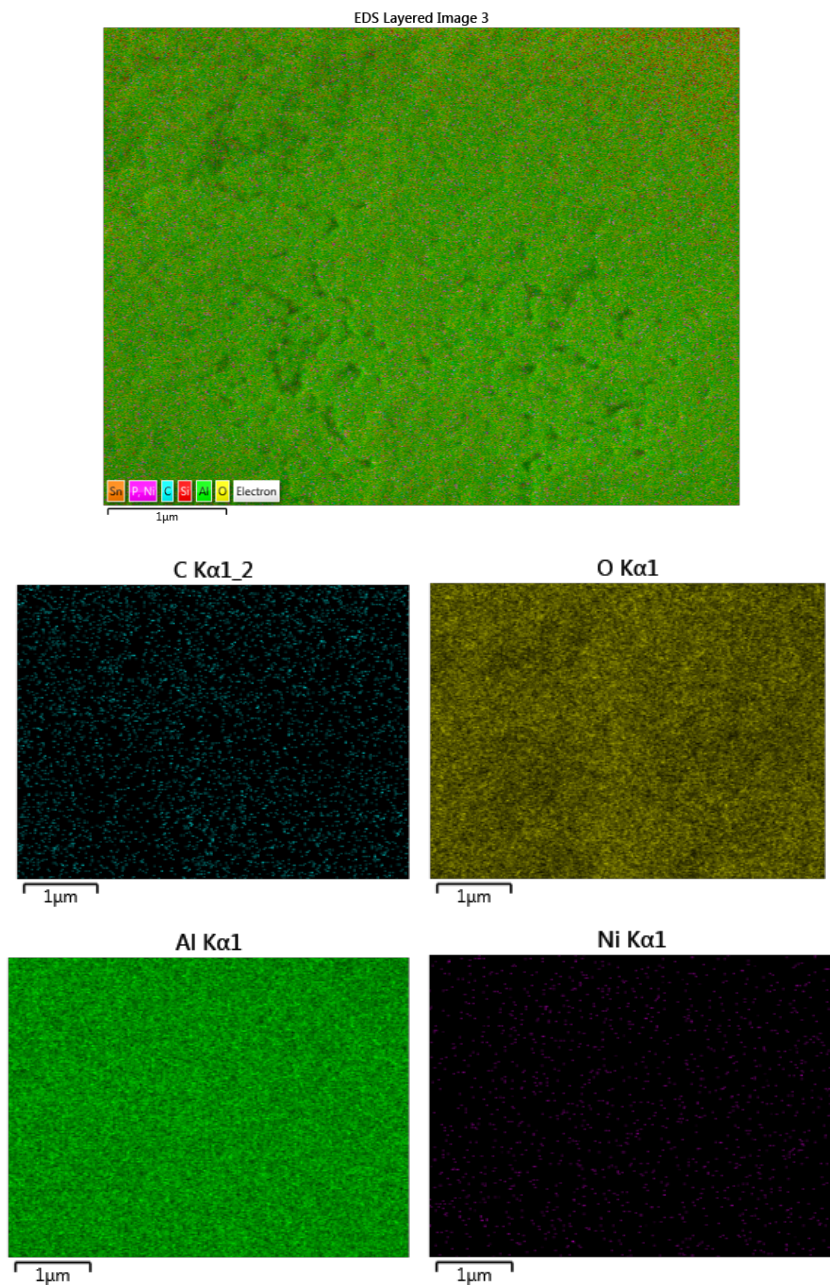


Fig 5.6 Elemental mapping of 100 nm coated alumina

Fig 5.6 shows that the nickel coating of 100 nm alumina also succeeds. And the nickel element distribution in fig 5.6 indicates that the coating of 100 nm alumina was uniform.

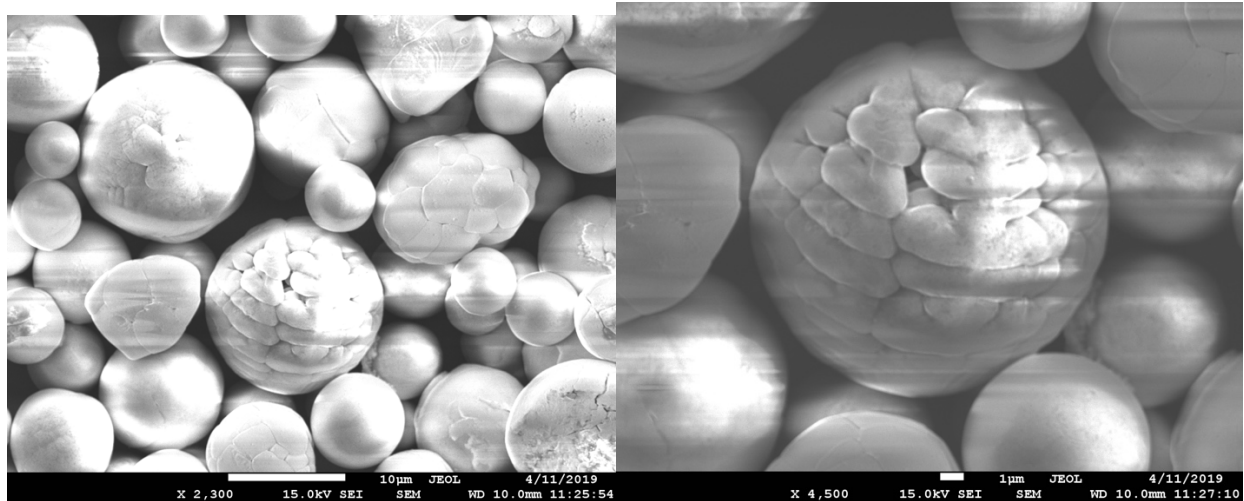


Fig 5.7 SEM micrograph of 10 μm coated alumina

Compare fig 5.7 with 10 μm uncoated alumina in fig 5.2 (c), we can observe texture on particle surface as uniform coating clearly.

5.1.2 Microstructure of consolidated SPS

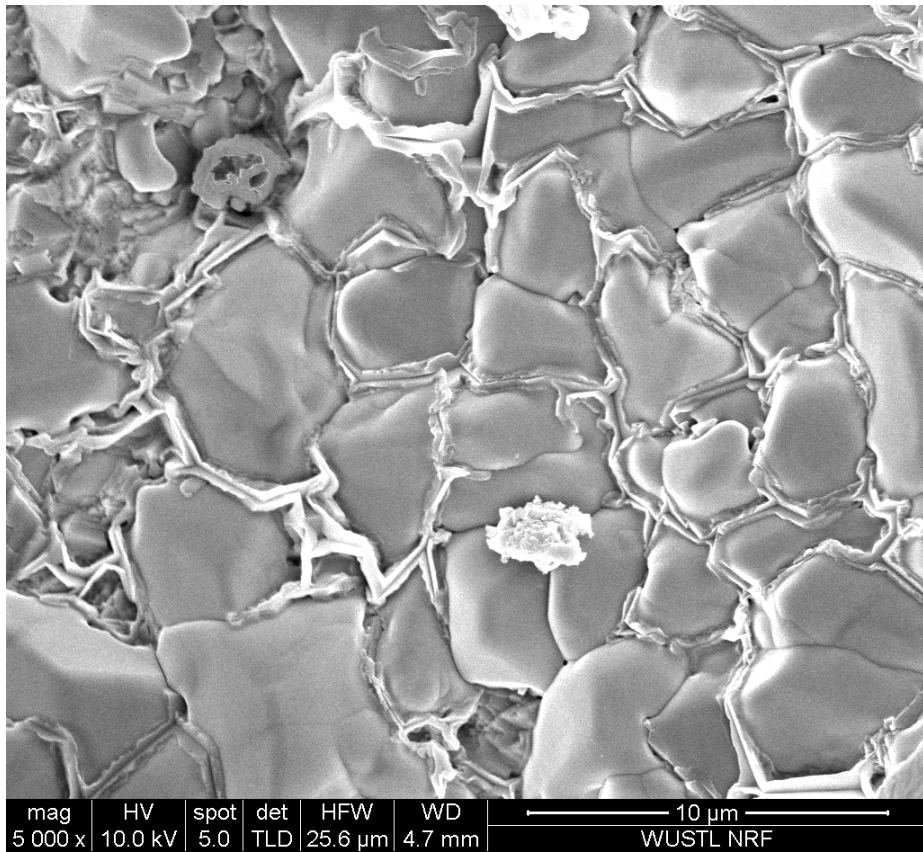


Fig 5.8 SEM micrograph of 100 nm coated alumina annealed for 10 hrs (magnification: 5000x)

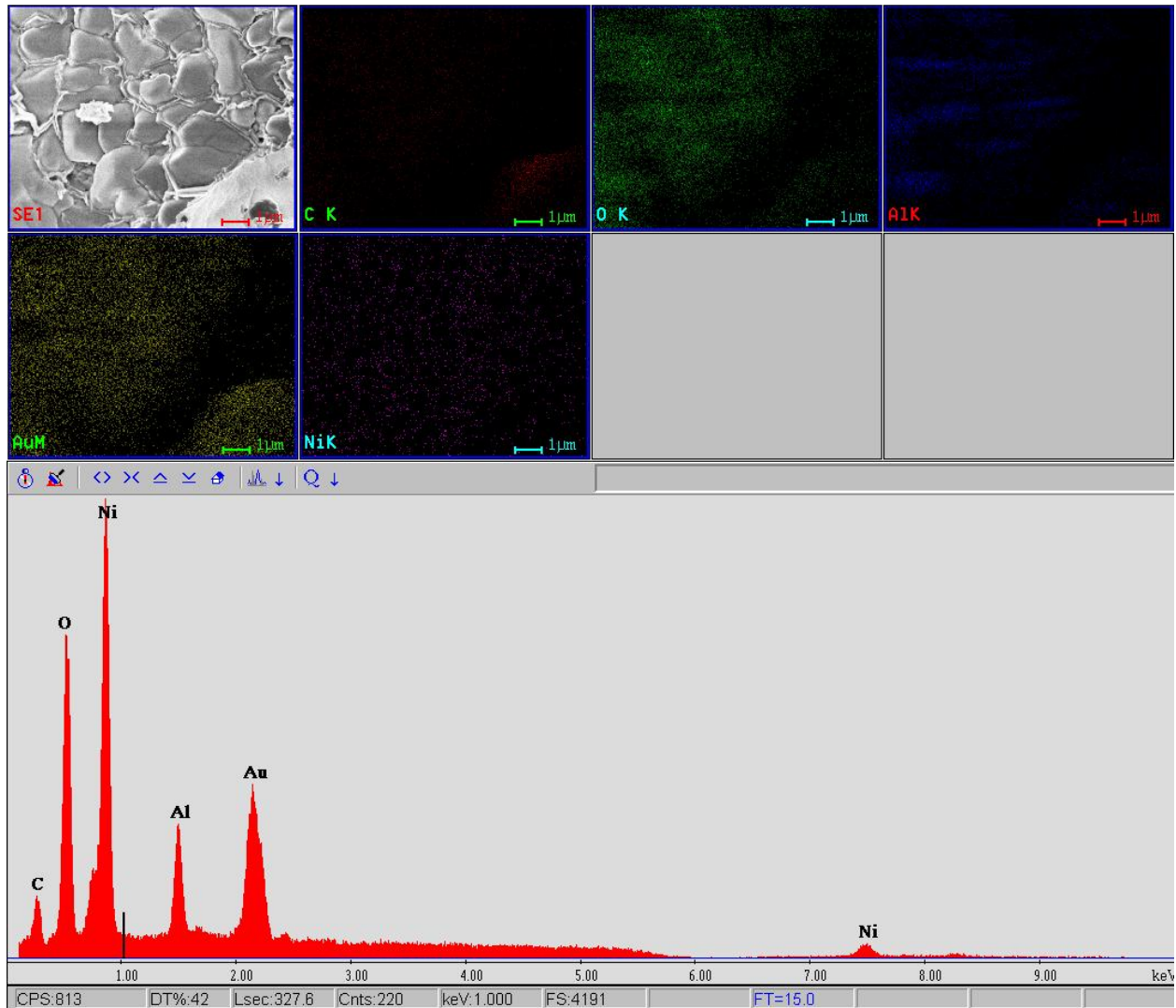


Fig 5.9 EDX spectrum and element distribution of 100 nm coated alumina annealed for 10 hrs

From fig 5.8, we can see the grain size increased to around $5 \mu\text{m}$ during the electroless nickel plating and spark plasma sintering process. And the uniform nickel plating is shown around the particle. And fig 5.9 is an evidence that support the information we got from fig 5.8. The nickel plating was successful and the coating was uniform.

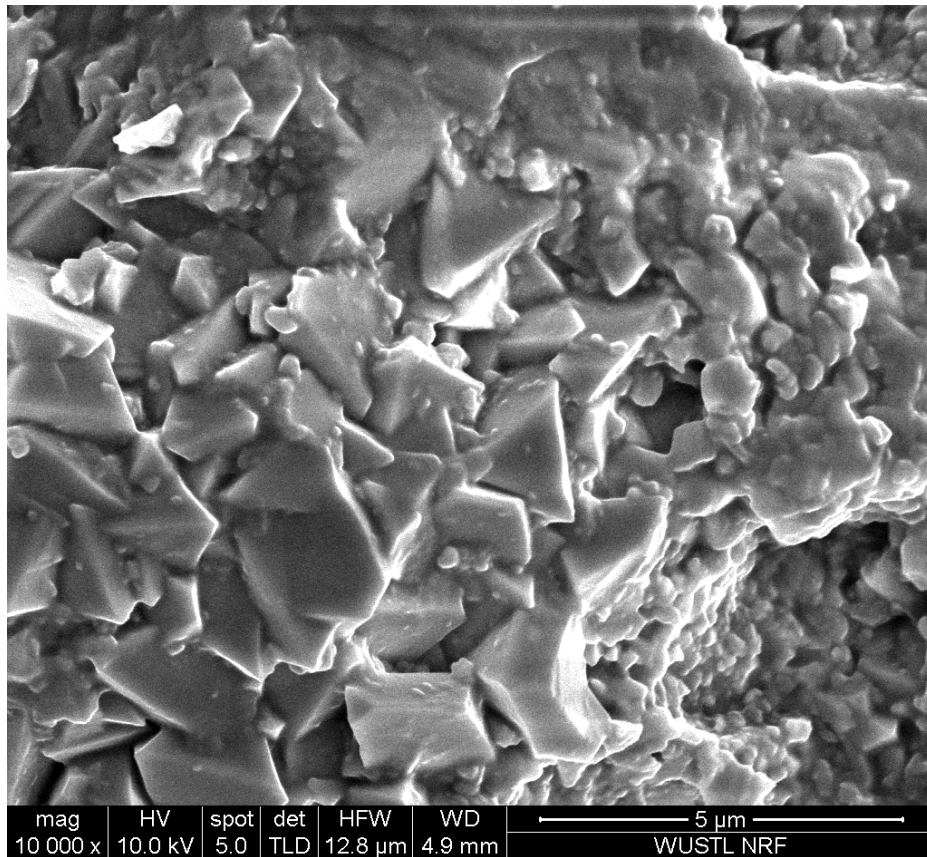


Fig 5.10 SEM micrograph of 100 nm coated alumina annealed for 1.5 hrs (magnification: 10000)

In fig 5.10, it shows the sintered 100 nm coated alumina annealed for 1.5 hours has few porous. And we can see some small grains in the right side of figure. That means our goal to improve fracture toughness by fine grain toughening is successful. And compare fig 5.10 with fig 5.8, we can conclude the better annealing time of coated alumina should be 1.5 hours.

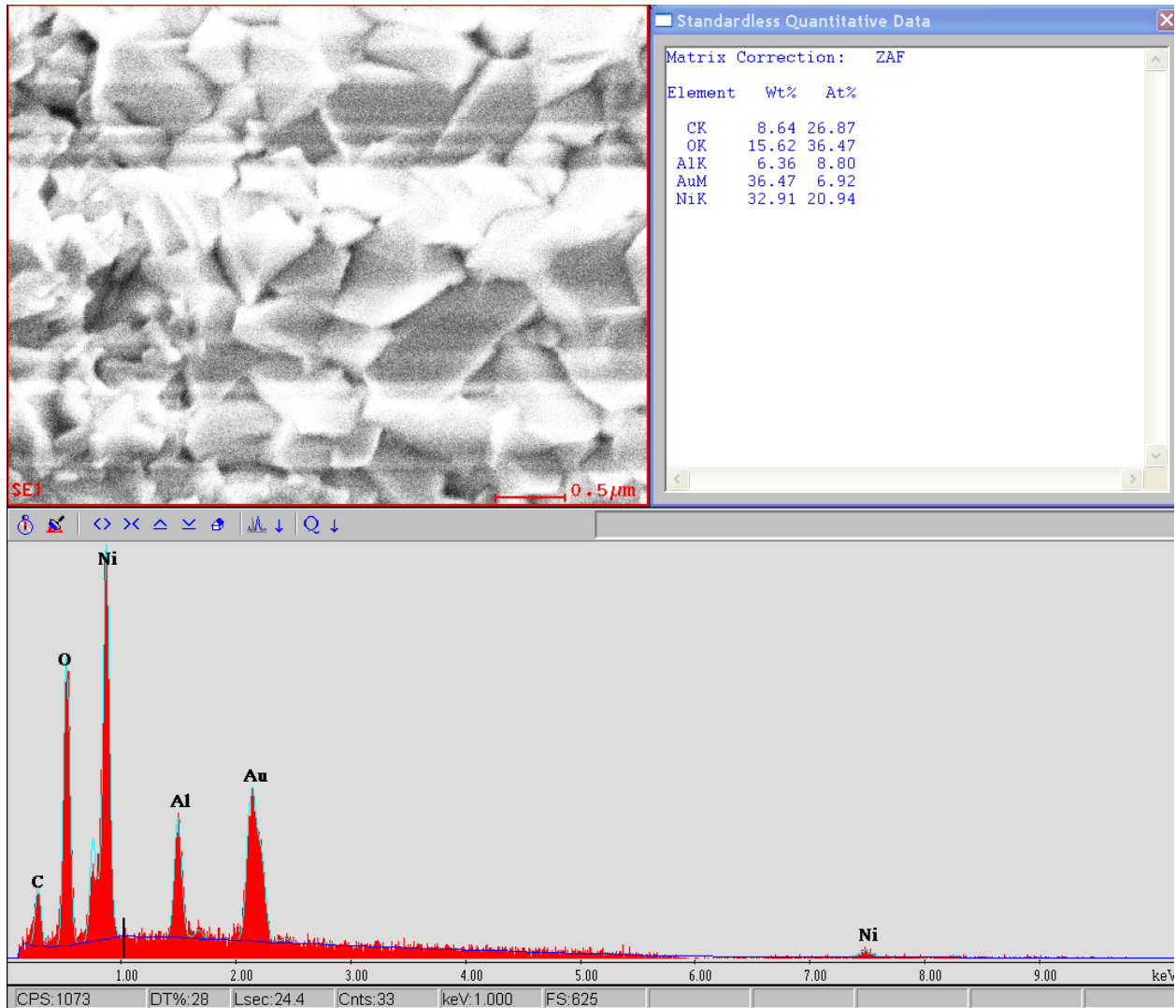
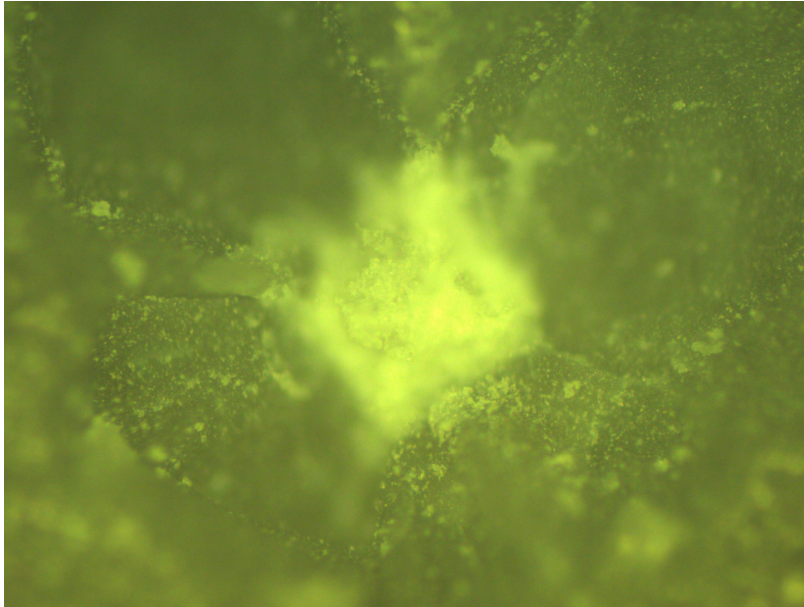


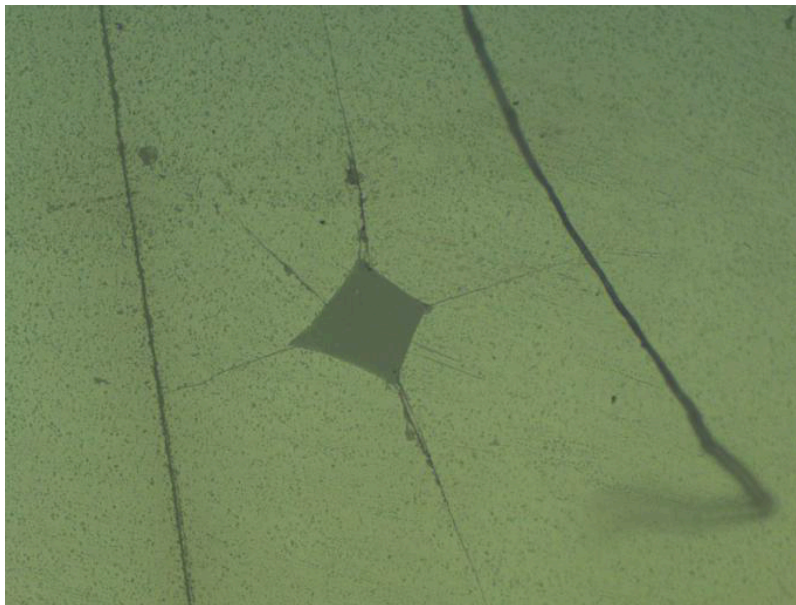
Fig 5.11 EDX spectrum of 100 nm coated alumina annealed for 1.5 hrs

5.2 Indentation

Fig 5.3 shows that the crack length is much longer for uncoated alumina than coated alumina. Both the two samples in figure 5.3 were 100 nm alumina sintered at 1325°C. Their indentation size and crack length shows that the coated alumina achieves higher fracture toughness without decrease the hardness of alumina.



(a)



(b)

Fig 5.12 (a) Optical micrograph of indentation of 100 nm coated alumina sintered at 1325°C

(b) Optical micrograph of indentation of 100 nm uncoated alumina sintered at 1325°C

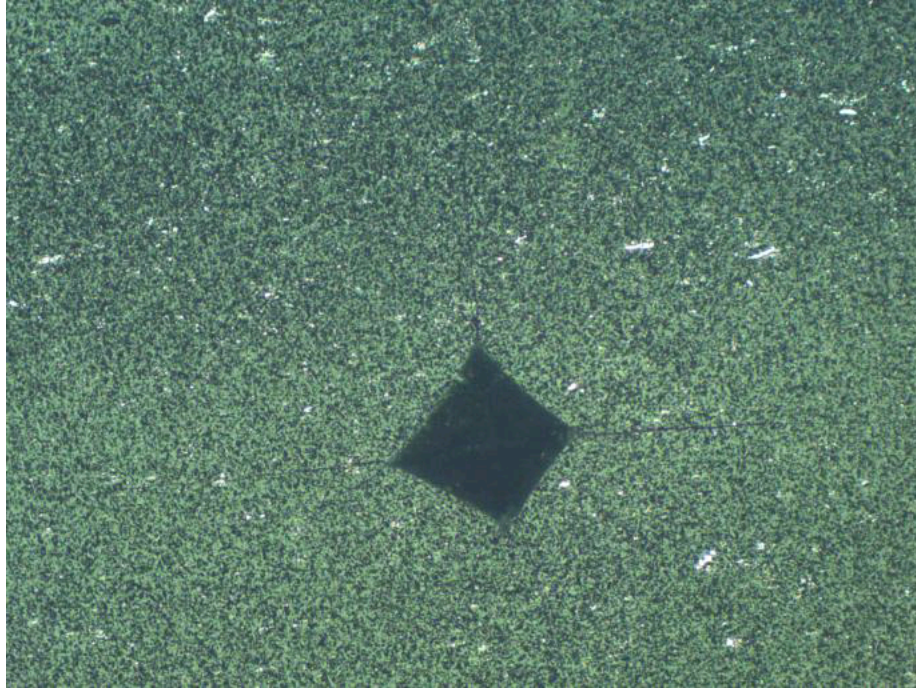


Fig 5.13 Optical micrograph of indentation of 100 nm coated alumina sintered at 1400 °C

From fig. 5.4 and fig. 5.3 (a), we can see the crack length is longer for coated alumina sintered at 1400 °C than coated alumina sintered at 1325 °C. It shows that 1325 °C should be a better sintering temperature for fracture toughness improvement for alumina based ceramics.

5.3 Densities

From a review of the literature of alumina based ceramics, the density of alumina is 3.95 **g/cm³** [35]. If we assume the alumina particle to be spherical, and the nickel plating is coated around the particle surface uniformly. The theoretical density of coated alumina should be 4.24 **g/cm³**, 4.50 **g/cm³**,

4.75 **g/cm³**, 4.97 **g/cm³** and 5.18 **g/cm³**, where the thickness of nickel plating is 1 nm, 2 nm, 3 nm, 4 nm and 5 nm. Our density of coated alumina measured by Archimedes method were from 2.88 **g/cm³** to 4.10 **g/cm³**. The lower density may cause by porous in consolidated sample. The density of all the consolidated samples are listed in table 5.1.

Table 5.1 Density of consolidated coated and uncoated alumina

Material	Density, g/cm^3
density of conventional uncoated alumina	3.95
Theoretical density of coated alumina with 1 nm nickel plating	4.24
Theoretical density of coated alumina with 2 nm nickel plating	4.50
Theoretical density of coated alumina with 3 nm nickel plating	4.75
Theoretical density of coated alumina with 4 nm nickel plating	4.97
Theoretical density of coated alumina with 5 nm nickel plating	5.18
100 nm coated alumina sintered at 1400 °C (annealed at 1100 °C for 10h)	3.87
100 nm coated alumina sintered at 1400 °C (annealed at 1100 °C for 1.5h)	3.77
100 nm coated alumina sintered at 1400 °C	3.75
100 nm uncoated alumina sintered at 1325 °C (annealed at 1100 °C for 10h)	3.58
100 nm uncoated alumina sintered at 1325 °C (annealed at 1100 °C for 1.5h)	3.79
100 nm uncoated alumina sintered at 1325 °C	3.61
100 nm uncoated alumina sintered at 1400 °C	3.97
100 nm coated alumina sintered at 1250 °C	3.53
100 nm coated alumina sintered at 1325 °C	3.60
100 nm coated alumina sintered at 1200 °C	2.88
0.5-1 μm coated alumina sintered at 1325 °C	4.1
100 nm coated alumina sintered at 1325 °C	3.82
10 μm uncoated alumina sintered at 1400 °C	3.58

Table 5.1 shows that the density of both coated and uncoated alumina was increased after annealing. The 100 nm coated alumina sintered at 1200 °C has density of 2.88, which is a lot lower than normal alumina. That indicates the sintering temperature of 1200 °C may be too low for coated alumina. And the highest density is 4.10 for 0.5-1 μm coated alumina sintered at 1325 °C. It shows that particle size of 0.5-1 μm might be the most suitable size for SPS to get fully densified consolidations.

5.4 Hardness

Uncoated alumina's hardness usually can be 14.71-16.18 GPa. Our hardness number of coated alumina vary from 6.29 GPa to 18.98 GPa when exclude an outlier, 22.32 GPa of coated 0.5-1 μm alumina sintered at 1325 °C. The decrease of hardness is expected for ductile phase reinforcement. The hardness of all coated and uncoated samples are listed in table 5.2.

Table 5.2 Hardness of coated and uncoated alumina

Material Hardness, GPa	1st	2nd	3rd	Avg.
Conventional alumina				14.71-16.18
100 nm coated alumina sintered at 1400 °C (annealed at 1100 °C for 10h)	11.26	9.186	7.896	9.45
100 nm coated alumina sintered at 1400 °C (annealed at 1100 °C for 1.5h)	8.318			8.318
100 nm coated alumina sintered at 1400 °C	11.39	11.97	11.57	11.64
100 nm uncoated alumina sintered at 1325 °C (annealed at 1100 °C for 10h)	16.64	16.59	16.36	16.53
100 nm uncoated alumina sintered at 1325 °C (annealed at 1100 °C for 1.5h)	20.35	17	19.6	18.98
100 nm uncoated alumina sintered at 1325 °C	16.52	16.75	17.04	16.77
100 nm coated alumina sintered at 1325 °C	16.8	15.43	18	16.74
100 nm coated alumina sintered at 1200 °C	6.093	6.477		6.285
0.5-1 μm coated alumina sintered at 1325 °C	24.41	23.22	19.33	22.32
100 nm coated alumina sintered at 1325 °C	11.13	7.17	8.985	9.095
10 μm uncoated alumina sintered at 1400 °C	6.461	6.248	6.465	6.39

5.5 Fracture Toughness

The minimum fracture toughness of alumina is $3.3 \text{ MPa}\cdot\sqrt{\text{m}}$. The maximum fracture toughness of alumina is $5 \text{ MPa}\cdot\sqrt{\text{m}}$. Our 100 nm uncoated alumina sintered at $1325 \text{ }^\circ\text{C}$ has fracture toughness of $5.05 \text{ MPa}\cdot\sqrt{\text{m}}$, increased 21.7% of the mean between $3.3 \text{ MPa}\cdot\sqrt{\text{m}}$ and $5 \text{ MPa}\cdot\sqrt{\text{m}}$ ($4.15 \text{ MPa}\cdot\sqrt{\text{m}}$). And fracture toughness of $10 \text{ }\mu\text{m}$ uncoated alumina sintered at $1400 \text{ }^\circ\text{C}$, $6.74 \text{ MPa}\cdot\sqrt{\text{m}}$, increased 62.4% of $4.15 \text{ MPa}\cdot\sqrt{\text{m}}$. So SPS could be an effective method for fracture toughness improvement. The 100 nm coated alumina sintered at $1325 \text{ }^\circ\text{C}$ has fracture toughness of $7.62 \text{ MPa}\cdot\sqrt{\text{m}}$ and $9.11 \text{ MPa}\cdot\sqrt{\text{m}}$, which are 33.7% and 80.4% higher than $5.05 \text{ MPa}\cdot\sqrt{\text{m}}$ of 100 nm uncoated alumina sintered at $1325 \text{ }^\circ\text{C}$. That means ENP improved fracture toughness of alumina ceramics effectively. The 100 nm coated alumina sintered at $1400 \text{ }^\circ\text{C}$ has fracture toughness of $4.44 \text{ MPa}\cdot\sqrt{\text{m}}$. The 100 nm coated alumina sintered at $1325 \text{ }^\circ\text{C}$ has fracture toughness of $9.11 \text{ MPa}\cdot\sqrt{\text{m}}$. The 100 nm coated alumina sintered at $1200 \text{ }^\circ\text{C}$ has fracture toughness of $3.95 \text{ MPa}\cdot\sqrt{\text{m}}$. Those results could be an indication that $1325 \text{ }^\circ\text{C}$ is the best sintering temperature for alumina. The fracture toughness of $0.5\text{-}1 \text{ }\mu\text{m}$ coated alumina sintered at $1325 \text{ }^\circ\text{C}$ is $9.22 \text{ MPa}\cdot\sqrt{\text{m}}$, which is 21% higher than $7.62 \text{ MPa}\cdot\sqrt{\text{m}}$, the fracture toughness of 100 nm coated alumina sintered at $1325 \text{ }^\circ\text{C}$. The fracture toughness of 100 nm uncoated alumina sintered at $1325 \text{ }^\circ\text{C}$ and coated alumina sintered at $1400 \text{ }^\circ\text{C}$ is $5.05 \text{ MPa}\cdot\sqrt{\text{m}}$ and $4.44 \text{ MPa}\cdot\sqrt{\text{m}}$. After annealing for 1.5 hours and 10 hours, the fracture toughness of uncoated alumina became $7.64 \text{ MPa}\cdot\sqrt{\text{m}}$ and $5.45 \text{ MPa}\cdot\sqrt{\text{m}}$. The fracture toughness of coated alumina became $7.85 \text{ MPa}\cdot\sqrt{\text{m}}$ and $6.59 \text{ MPa}\cdot\sqrt{\text{m}}$. This result shows that the post SPS annealing results an increase in toughness values of alumina ceramics.

Table 5.3 Fracture toughness of all uncoated and coated samples

Material Fracture Toughness, $\text{MPa}\cdot\sqrt{\text{m}}$	1st	2nd	3rd	Avg.
Conventional alumina				3.5
100 nm coated alumina sintered at 1400 °C (annealed at 1100 °C for 10h)	3.15		10.02	6.585
100 nm coated alumina sintered at 1400 °C (annealed at 1100 °C for 1.5h)	7.85			7.85
100 nm coated alumina sintered at 1400 °C	6.28	3.83	3.21	4.44
100 nm uncoated alumina sintered at 1325 °C (annealed at 1100 °C for 10h)	4.91	7.51	3.93	5.45
100 nm uncoated alumina sintered at 1325 °C (annealed at 1100 °C for 1.5h)	8.04	6.77	8.12	7.64
100 nm uncoated alumina sintered at 1325 °C	4.7	6.47	3.98	5.05
100 nm coated alumina sintered at 1325 °C	9.19	6.42	11.73	9.11
100 nm coated alumina sintered at 1200 °C	4.32	3.58		3.95
0.5-1 μm coated alumina sintered at 1325 °C	10.38	9.2	8.09	9.22
100 nm coated alumina sintered at 1325 °C	7.05	6.12	9.68	7.62
10 μm uncoated alumina sintered at 1400 °C	6.74			6.74

Chapter 6

Summary and Conclusions

The principal conclusions of our study are:

- Ductile Nickel coating was achieved on nano alumina particle surface.
- Grain size variations were obtained by selecting different sizes of alumina particles and by post consolidation annealing.
- Optimum conditions for best combination of density, hardness and fracture toughness were determined.
- Spark plasma sintering of nickel coated 100-10000 nm alumina particles is shown to be a viable approach for toughening of alumina ceramics.
- SPS slightly increase the hardness of uncoated alumina ceramics, and the best sintering temperature among the temperature we tried is 1325 °C.
- Post SPS annealing influence fracture toughness positively and the best annealing time is 1.5 hours,.
- Fracture toughness increase by with decreasing grain size.
- ENP is an effective method for ductile phase reinforcement.

Chapter 7

Future Work

- More variations in particle size and sintering temperature should be investigated.
- Effects of post consolidation annealing variations – temperature and time on the resulting density, hardness, and fracture toughness should be investigated.
- Other mechanical properties, such as bend strength at room temperature and high temperature creep should be investigated to enhance the application of coated alumina ceramics.
- Grain size control and ductile phase reinforcement should be generalized to other ceramics, such as Zirconia, Titania, Tungsten Carbide.

References

- [1] Z. Y. Deng, T. Fukasawa, M. Ando, G. J. Zhan, T. Ohji, High-surface-area alumina ceramics fabricated by the decomposition of $\text{Al}(\text{OH})_3$, *J. Am. Ceram. Soc.* 84 (2001) 485-491.
- [2] D. Hardy, D. J. Green, Mechanical properties of a partially sintered alumina, *J. Eur. Ceram. Soc.* 15 (1995) 769-775.
- [3] Z. Y. Deng, J. F. Yang, Y. Beppu, M. Ando, T. Ohji, Effect of agglomeration on mechanical properties of porous zirconia fabricated by partial sintering, *J. Am. Ceram. Soc.* 85 (2002) 1961-1965.
- [4] S. F. Corbin, P. S. Apye, Engineered porosity via tape casting, laminatin and the percolation of pyrolyzable particulates, *J. Am. Ceram. Soc.* 82 (1999) 1693-1701.
- [5] J. L. Han, F. Saito, B. T. Lee, Microstructures of porous Al_2O_3 -50 wt% ZrO_2 composites using in-situ synthesized $\text{Al}_2\text{O}_3 - \text{ZrO}_2$ composite powders, *Mater. Lett.* 58 (2004) 2181-2185.
- [6] M. M. Aleksyuk, A method for the strength prediction of porous ceramics, *Strength Mater.* 33 (2001) 188-192.
- [7] Tokita, M., Trends in Advanced SPS Spark Plasma Sintering System and Technology, *J. Soc. Powder Technol. Jpn.*, 30 [11] 790-804 (1993).
- [8] Risbud, S. H., Shan, C. H., Mukherjee, A. K., Bow, J. S., and Hall, R. A., Retention of Nanostructure in Aluminum Oxide by Very Rapid Sintering at 1150°C, *J. Mater. Res.*, 10 [2] 237-9 (1995).
- [9] V. Carle, B. Trippel, U. Taffner, U. Schafer, F. Predel, R. Telle, and G. Petzow, Ceramography of High Performance Ceramics: Description of the Materials, Preparation, Etching Techniques, and Description of the Microstructure—Part VIII, Aluminum Oxide, *Pract. Metallogr.*, Vol 32, 1995, p 54-76.
- [10] U. Schafer, H. Schubert, V. Carle, U. Taffner, F. Predel, and G. Petzow, Ceramography of High Performance of Ceramics: Description of the Materials, Preparation, Etching Techniques, and Description of the Microstruture—Part III, Zirconium Oxide, *Pract. Metallogr.*, Vol 28, 1991, p 468-483.

- [11] J. Chevalier, L. Gremillard, *Ceramics for Medical Applications: A Picture for the Next 20 Years*, 2008 1-2
- [12] S. Zinelis, W. Brantley, *Structure/property relationships in orthodontic ceramics*, in *Orthodontic Applications of Biomaterials*, 2017
- [13] V.D. Krstic and A.K. Khaund" *Advances in Fracture Research*, Proc. 5th Int. Conf. on Fracture, D. Francois, C. Bathias, B.A. Bilby, Y. D'Escatha, J. Knott, R. Labbeus, T.C. Lindley, A. Pelissier-Tanon, P. Petrequin, A. Pineau, J. Poirier, G. Sanz, E. Sommer, and L.E. Steele, eds., Pergamon Press, New York, NY, 1981, pp. 1577-85.
- [14] V.D. Krstic, P.S. Nicholson, and R.G. Hoagland: *J. Am. Ceram. Soc.*, 1981, vol. 64, pp. 499-504.
- [15] V.D. Krstic, P.S. Nicholson, and R.G. Hoagland: *J. Am. Ceram. Soc.*, 1981, vol. 64, pp. 499-504.
- [16] M.F. Ashby, F.J. Blunt, and M. Bannister: *Acta Metall.*, 1989, vol. 37, pp. 1847-57.
- [17] C.K. Elliott, G.R. Odette, G.E. Lucas, and J.W. Sheckherd: in *High-Temperature~High-Performance Composites*, MRS Syrup. Proc., F.D. Lemkey, A.G. Evans, S.G. Fishman, and J.R. Strife, eds., MRS, Pittsburgh, PA, 1988, vol. 120, pp. 95-101.
- [18] H.E. Drove, A.G. Evans, G.R. Odette, R. Mehrabian, M.L. Emiliani, and R.J. Hecht: *Acta Metall. Mater.*, 1990, vol. 38, pp. 1491-1502.
- [19] G.R. Odette, H.E. D~ve, C.K. Elliott, A. Harigowa, and G.E. Lucas: in *Interfaces in Ceramic Metal Composites*, R.J. Arsenault, R.Y. Lin, G.P. Martins, and S.G. Fishman, eds., TMS-AIME, Warrendale, PA, 1990, pp. 443-63.
- [20] H.C. Cao, B.J. Dalgleish, H.E. D~ve, C. Elliott, A.G. Evans, R. Mehrabian, and G.R. Odette: *Acta Metall.*, 1989, vol. 37, pp. 2969-77.
- [21] T.C. Lu, A.G. Evans, R.J. Hecht, and R. Mehrabian: *Acta Metall. Mater.*, 1991, vol. 39, pp. 1853-62.
- [22] B.D. Flinn, M. R0hle, and A.G. Evans: *Acta Metall.*, 1989, vol. 37, pp. 3001-06.
- [23] P. Hing and G.W. Groves: *J. Mater. Sci.*, 1972, vol. 7, pp. 427-34.
- [24] L.S. Sigl and H.E. Exner: *Metall. Trans. A*, 1987, vol. 18A, pp. 1299-1308.

- [25] S.M. Pickard and A.K. Ghosh: Metall. Mater. Trans. A, 1996, vol. 27A, pp. 909-21.
- [26] Sudagar, Jothi; Lian, Jianshe; Sha Wei, Electroless Nickel, Alloy, Composites and Nano coatings-A Critical Review, Journal of Alloys and Compounds, 571, 2013, p 183-204.
- [27] Mordechay Schlesinger, Milan Paunovic, Electroless Deposition of Nickel, 2010
- [28] J. Kisel, Ph.D. Thesis, University of Windsor (1988); M. Schlesinger and J. Kisel, J. Electrochem. Soc, 136, 1658 (1989).
- [29] J. E. A. M. Van den Meerakker, J. Appl. Electrochem., 11, 395 (1981).
- [30] M. Tokita 'PM' 2000: World Congress on Powder Metallurgy, 729-732; 2000, Tokyo, Japan Society of Powder and Powder Metallurgy.
- [31] G. Petzow, Metallographic Etching, 2nd ed., ASM International, 1999
- [32] V. Carle, U. Schäfer, U. Täffner, F. Predel, R. Telle, and G. Petzow, Ceramography of High Performance Ceramics: Description of the Materials, Preparation, Etching Techniques, and Description of the Microstructure—Part I, Ceramographic Etching, Pract. Metallogr., Vol 28, 1991, p 359–377.
- [33] Ulrike Täffner, Veronika Carle, and Ute Schäfer, Max-Planck-Institut für Metallforschung, Stuttgart, Germany Michael J. Hoffmann, Institute für Keramik im Maschinenbau, Universität Karlsruhe, Germany, Preparation and Microstructural Analysis of High-Performance Ceramics, 2004, p 3-5.
- [34] Evans A. G. and Charles E. A. (1976). Fracture Toughness Determination by Indentation, J. Am. Ceram. Soc., Vol. 59, (1976), pp. 371-372.
- [35] Material Properties Data: Alumina (Aluminum Oxide) Archived 2010-04-01 at the Wayback Machine.